International Scholarly Research Network
ISRN Nanotechnology
Volume 2011, Article ID 759838, 9 pages
doi:10.5402/2011/759838

Research Article

A Comparative Study of Optical Anisotropies of BC_3 and B_3C Systems by Density Functional Theory

Debnarayan Jana,[1] Li-Chyong Chen,[2] Chun Wei Chen,[3] and Kuei-Hsien Chen[2,4]

[1] *Department of Physics, University of Calcutta, West Bengal, Kolkata 700 009, India*
[2] *Center for Condensed Matter Sciences, National Taiwan University, Taipei 10617, Taiwan*
[3] *Department of Material Science and Engineering, National Taiwan University, Taipei 10617, Taiwan*
[4] *Institute of Atomic and Molecular Sciences, Academia Sinica, Taipei 10617, Taiwan*

Correspondence should be addressed to Debnarayan Jana, cujanad@yahoo.com

Received 11 April 2011; Accepted 14 May 2011

Academic Editors: B. Coasne and J.-J. Kim

The optical properties of (8,0) BC_3 and B_3C single-wall carbon nanotubes (SWCNTs) are computed using *ab initio* density functional theory (DFT). The electronic band structure reveals that the Fermi energy of B_3C system is reduced compared to BC_3. The static dielectric constant in the long wavelength limit for B_3C system is 9 times larger than that of BC_3 in unpolarized electromagnetic field. Within 10 eV frequency (energy) range, the absorption coefficient of B_3C is higher compared to BC_3, while, above 10 eV, it is less than that of BC_3. In parallel polarization, the peak of the loss function for B_3C is shifted to higher frequency (energy) region with significantly six orders of magnitude compared to BC_3 system. The analysis of this study indicates that the optical anisotropies can be gained easily in these boron-doped systems by appropriately choosing the direction of the polarization of the electromagnetic field. Besides, the results of the loss functions may throw some light on the nature of collective excitations of these two systems.

1. Introduction

From its very discovery in 1991, carbon nanotubes (CNTs), both single wall as well as multiwall, have attracted the attention of theoretical and experimental research groups [1, 2]. Due to their unique one-dimensional structure and unusual electronic properties, they can be regarded as one of the natural building blocks of molecular electronics. Single-wall carbon nanotubes (SWCNTs) consist of a single graphene layer rolled on a cylinder with diameters between 1 and 2 nm having lengths of the order of few hundred micrometers. The calculations reveal that their electronic properties can be semiconducting, metallic, or quasimetallic depending on their geometrical structure dictated by a quantity known as the chirality. The optical properties of 4 Å diameter pure SWCNT have been investigated [3–5] recently by first principles calculation to explain the experimental results. Most recently, *ab initio* calculations of the linear and nonlinear optical properties of pure CNTs have shown that the dielectric function depends essentially on chirality, diameter and the nature of polarizations of incident electromagnetic field [6].

The electronic properties of single-wall carbon nanotubes (SWCNTs) can be tailored [7, 8] by substituting carbon atom(s) by heteroatom (s) such as boron or nitrogen. It is well known that pure CNTs are unable to detect highly toxic gases, water molecules, and biomolecules [9]. To improve the nanosensor reliability and quality, the importance of substitution alloying of impurity atoms such as boron and nitrogen has been discussed [10]. In fact, a calculation on the chemical interaction reveals that the boron doped CNT can act as a novel sensor [11] for formaldehyde. The synthesis of composite $B_xC_yN_z$ tubes has been performed and their energy loss spectroscopy have been reported [12, 13]. In general, through the reaction of B_2O_3 with CNTs under an Ar atmosphere [14], B atom(s) can be substituted for the carbon atom(s) of SWNT. In the literature, the synthesis and electronic properties of B-substituted SWCNT have been discussed [15, 16]. A quantum chemical calculation [17] has been employed to

investigate the larger mobility (i.e., electronic conductivity) of B- and N- doped CNTs. Recently, the electronic structure and optical properties of B- doped single-wall carbon nanotubes (SWCNTs) have been studied in detail, and it is found that boron is in sp^2 configuration [18]. It has also been shown recently that even a small amount dopant can significantly change the mesoscopic conductivity [19] of chemically B-doped CNTs. The electron current distribution in B- and N-doped armchair CNT has been investigated [20] using Density Functional Theory [DFT] and Green's function to show a chiral flow of current. All the above examples eventually indicate the importance of the study of B-doped CNTs and invite further investigation about the optical properties of the doped system as a function of B concentration. Since this doping can alter the band structure of SWCNTs (such as band gap, the density of states near Fermi energy) considerably [21, 22], we would naturally expect some dramatic changes in the response of the B_xC_y nanotubes under an electromagnetic field. As a matter of fact, in recent years the spectroscopic studies of BC_3 SWNTs have been interpreted in terms of *ab initio* band structure calculation [23, 24].

With this motivation, we are interested in computing the optical properties of these two boron-doped systems in different polarizations of the electromagnetic field. In particular, in this paper, we study the optical response of (8,0) BC_3 and B_3C SWCNTs under the action of a uniform electric field with various polarizations direction through relaxed C-C bond length *ab initio* (DFT) calculations in the long wavelength limit. The geometrical structures of these systems were built by replacing some of the carbon atom(s) in the hexagonal ring by B atoms. The preferred boron sites were chosen having lowest total energy.

2. Computational Methods

The numerical methods are employed using first-principles (DFT) with Generalized Gradient Approximation (GGA) as implemented in CASTEP code [25] in the materials studio and simulation software package. Using this method, we calculate the dielectric constant and other related optical properties such as absorption coefficients, reflectivity, and the loss function. The last three quantities are however experimentally accessible. An extensive thorough account of the numerical computation dealing with B-alloyed system has been described in our earlier work [26–28].

The optical properties of any system are generally studied by the complex dielectric function defined by $\vec{D}(\omega) = \varepsilon(\omega)\vec{E}(\omega) = [\varepsilon_1(\omega) + i\varepsilon_2(\omega)]\vec{E}(\omega)$. However, $\varepsilon_1(\omega)$ and $\varepsilon_2(\omega)$ are not independent of each other. Within the framework of time dependent perturbation theory along with simple dipole approximation used in CASTEP code [25], the imaginary part is given by

$$\varepsilon_2(q \longrightarrow 0_{\vec{u}}, \hbar\omega) = \frac{2e^2\pi}{\Omega\varepsilon_0} \sum_{k,v,c} \left| \left\langle \psi_k^c | \vec{u} \cdot \vec{r} | \psi_k^v \right\rangle \right|^2 \times \delta\left(E_k^c - E_k^v - E\right), \tag{1}$$

where Ω and ε_0 represent, respectively, the volume of the supercell and the dielectric constant of the free space. It is easy to notice that the expression in (1) is similar to Fermi's Golden rule for time-dependent perturbation in quantum theory. Physically speaking, $\varepsilon_2(\omega)$ can be visualized as a parameter concerning the real transitions between the occupied valence band (VB) and unoccupied electronic states. The vector $\vec{u}$ defines the state of polarization of the incident electric field while $\vec{r}$ is the position vector. The sum over k is a crucial point in such numerical calculations. It actually samples the whole region of Brillouin zone (BZ) in the k space by taking a symmetrized Monkhorst-Pack [29] grid and smearing each energy level with a Gaussian spread function. The other two sums take care of the contribution of the unoccupied conduction band (CB) and occupied valence band (VB). In computing the above dielectric function, typically [(12) (total number of electrons +4)] number of bands were taken. No phonon contribution was taken here. Moreover, in this formulation, the local field effect and the excitonic effect have been neglected. The atomic positions are relaxed until the forces on the atoms are less than 0.01 eV/Å. The typical convergence was achieved till the tolerance in the Fermi energy is 0.1×10^{-6} eV. After checking the convergence, for sampling the irreducible part of the Brillouin Zone (BZ), we have used $(2 \times 2 \times 5)$ Monkhorst and Pack mesh having 6 k points with a cut-off energy of 470 eV. The smearing broadening in computing the optical properties was kept fixed at 0.5 eV.

The matrix element described in (1) for the electronic transition is computed between the single-electron energy eigenstates. To determine the wave functions in (1), we perform the first-principles spin unpolarized density functional theory using plane wave pseudopotential methods [30, 31]. Like any *ab initio* calculation, the self-consistent Kohn Sham (KS) equation has been employed here to compute the eigen function. For the exchange and correlation term, the generalized gradient approximation (GGA) as proposed by Perdew-Berke-Ernzerhof [32] is adopted. The standard norm-conserving pseudo-potential in reciprocal space is invoked for the optical calculation. Because of using of nonlocal potentials in this software, the matrix elements are modified as

$$\left\langle \psi_k^c \left| \vec{r} \right| \psi_k^v \right\rangle = \frac{1}{im\omega} \left\langle \psi_k^c \left| \vec{p} \right| \psi_k^v \right\rangle + \frac{1}{\hbar\omega} \left\langle \psi_k^c \left| \left[V_{\mathrm{nl}}(\vec{r}), \vec{r} \right] \right| \psi_k^v \right\rangle. \tag{2}$$

In comparison with the standard local density approximation (LDA) (with appropriate modifications) used mostly in electronic band structure calculation, the optical properties of the system are normally standardized by *spin unpolarized* GGA.

The typical computational supercell used here is the 3D triclinic crystal (a = 18.801 Å, b = 19.004 Å, c = 4.219 Å, and angles $\alpha = \beta = 90°, \gamma = 120°$) having symmetry P1. The supercells are built by taking four units of CNT. The energy cut-off, k-point sampling, geometry, GGA/norm-conserving pseudopotential are the same in these two systems as well

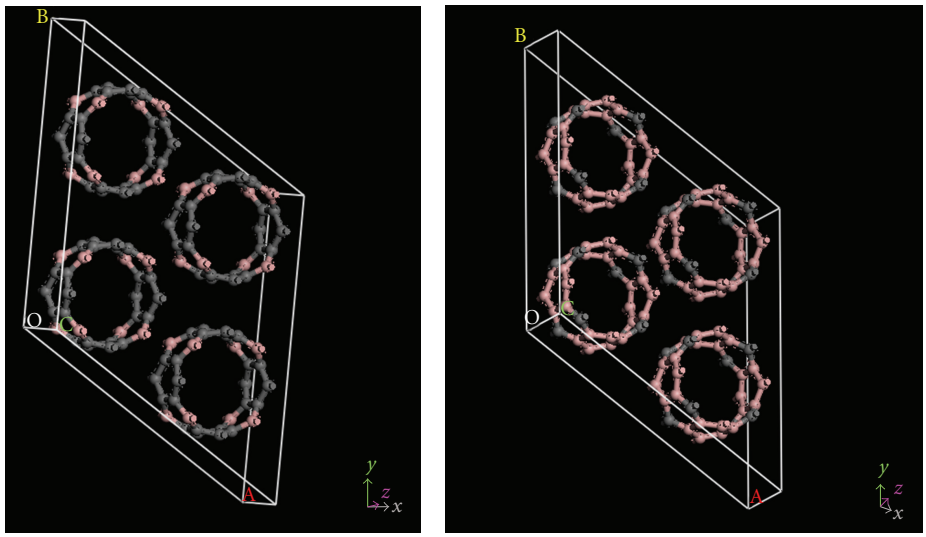

(a) (b)

Figure 1: Ball and stick model of (8,0) (a) BC_3 and (b) B_3C tube in 3D triclinic structure.

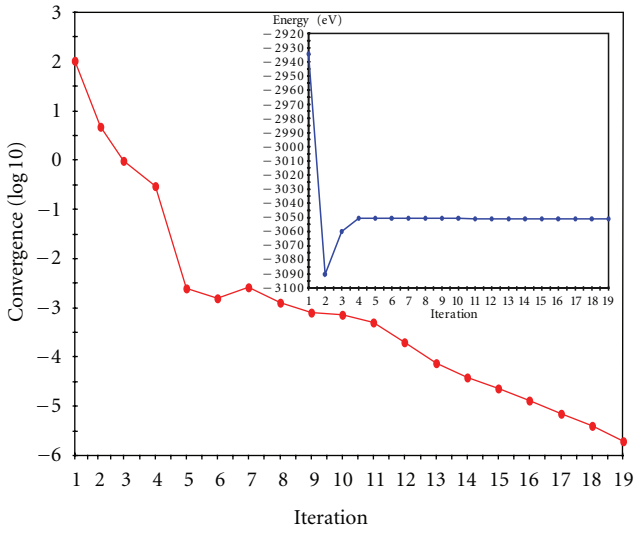

Figure 2: Typical energy change per atom of B_3C system. The convergence of the energy is noticed in the inset.

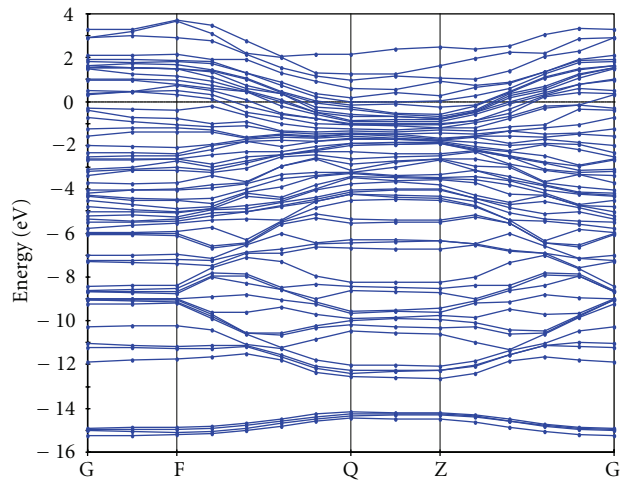

Figure 3: Typical band structure of B_3C systems. The dashed line indicates the position of the Fermi energy level.

as the pristine one. The anisotropic behavior in the optical properties can be investigated by taking into account the polarization vector $\vec{u}$ of the electromagnetic field in (1). Thus, the dielectric constant can be evaluated for three separate cases: one can choose in the direction of $\vec{u}$ (i) of electric field vector for the light at normal incidence (polarized); (ii) choosing $\vec{u}$ in the direction of propagation of incident light at the normal incidence but the electric field vector is considered as an average over the plane perpendicular to this direction (unpolarized); (iii) choosing $\vec{u}$ not in specified direction while the electric field vectors are taken as full isotropic average (polycrystalline). The directions of the field (k wave vector) have been chosen with respect to axis of the B-doped carbon nanotubes. The parallel polarization refers to $k(0,0,1)$ while perpendicular one $k(1,0,0)$.

3. Numerical Results and Discussions

3.1. Study of Band Structure of B_3C and BC_3 Systems. Before we discuss the optical properties, we show in Figure 1 the typical ball and stick model of (8,0) BC_3 and B_3C systems.

All the results presented in this paper have the same set of parameters as indicated in earlier section. For pure (8,0) we find the Fermi energy 6.028 eV with band gap at Γ point (most symmetric point in the BZ) as 0.48 eV. However, alloying with boron atoms in (8,0) nanotubes such as in BC_3 system, the Fermi energy reduces to 4.256 eV. With increasing

Table 1: Comparison of electronic and optical properties of BC_3 and B_3C systems.

Physical properties	BC_3	B_3C	Pristine
Fermi energy	4.25 eV	3.61 eV	6.03 eV
	38.45 (Un)	346.58 (Un)	19.82 (Un)
Static real dielectric constant	21.71 (Perp)	76.80 (Perp)	11.66 (Perp)
	33.26 (Para)	396.71 (Para)	30.98 (Para)
Absorption coefficient	Lower	Higher	Highest
Loss function	Lower (7–12 eV) (Un)	Higher in the same Range (Un)	Higher than BC_3 but lower than B_3C (Un)
Reflectivity	Smaller (Para)	Larger (Para)	Higher than BC_3 but very close to B_3C (Para)

(Un: unpolarized, Perp: perpendicular, Para: parallel).

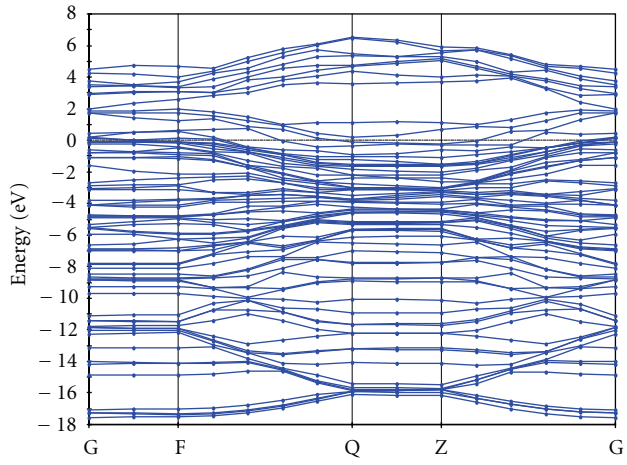

Figure 4: Typical band structure of BC_3 system.

more number of boron atoms in SWNTs, we find, for (8,0) B_3C nanotubes, a further reduction of the Fermi energy to 3.614 eV. More interestingly, we note a significant increase of the overlapping of valence and conduction band compared to pure as well as BC_3 SWNT. This is understood simply from the fact that the electronic configuration of B atom is $1s^2\ 2s^2 2p^1$.

Therefore, doping by B atom always reduces the total number of electrons N_0 in the system which on the other hand implies the decrease of Fermi energy with B doping. This has also been observed in boron doped multiwalled carbon nanotubes [33, 34]. In Figure 2, we show the typical number of self-consistent field (SCF) iterations and the convergence of the typical energy per atom of B_3C system.

In Figure 3, we schematically show the band structure of B_3C system, respectively. All the energies shown in the diagram have been measured with respect to the Fermi energy (shown as the dashed line in the band diagram). The most symmetric point ($k_x = k_y = k_z = 0$) is known as Γ point and is denoted by G in the energy band diagram. The band gap in BC_3 system turns out as 0.43 eV at Γ point, which is smaller than the pure one.

However, for B_3C system, the band gap turns out as 0.58 eV at Γ point, which is larger than the pure one. This engineering of band gap at the most symmetric point in BZ may be useful in device and sensor applications. These observations are required later on to understand some of the features of the optical properties of the doped CNT systems. The band structure shown in Figure 3 reveals that near the bottom of the valence band, there is a gap in energy for all values of k points in BZ. With increase of B doping, this feature is seen to be an integral part of the dispersion relation.

Apart from the difference of the Fermi energy in the two cases (see Table 1), the striking difference lies in the energy ranges between −12 eV and −14 eV. There exist energy states in BC_3 system while those are absent in the energy spectra in the VB for all values of k. Besides, it is clear from the two energy band diagrams (Figures 3 and 4) that the band width is higher in BC_3 compared to B_3C one.

The partial density of states (PDOS) of B atoms of (8,0) BC_3 and B_3C carbon nanotubes shown in Figure 5 indicates a series of spikes in the whole spectrum of band energy and these are basically the van Hove singularity typical characteristics of low-dimensional condensed matter systems. The low temperature scanning tunneling spectroscopy (STS) measurement can be used to verify the position of the spikes. It is seen that, in both pure and doped case, the contribution of p electrons in valence band is higher compared to its counterpart s electrons. However, the contribution of s electrons in both of the cases in the conduction band is meagre. In B_3C case, the contribution of p electrons at the Fermi level have been increased substantially compared to pure case. In fact, the higher value of DOS at the Fermi level signifies the metallicity character of B_3C. The DOS at the Fermi level is a measure of available free charge carriers. Thus, the increase of the DOS at the Fermi levels is a signature of more metallic character of B_3C system compared to BC_3 one.

The direction with relatively flat dispersionless bands at various k-points seems to contribute significantly to the optical absorption and hence allows one to explain the anisotropy of the optical properties. This is due to the fact that at those k values the group velocity of the electronic states vanishes with increase of DOS. Hence, an increase of the value of ε_2 is expected.

3.2. Study of Dielectric Constant of BC_3 and B_3C Systems. We compute the imaginary part of the dielectric constant within the specified frequency range. The polarizations of the electromagnetic field play an important role in computing the imaginary part of the dielectric constant. We

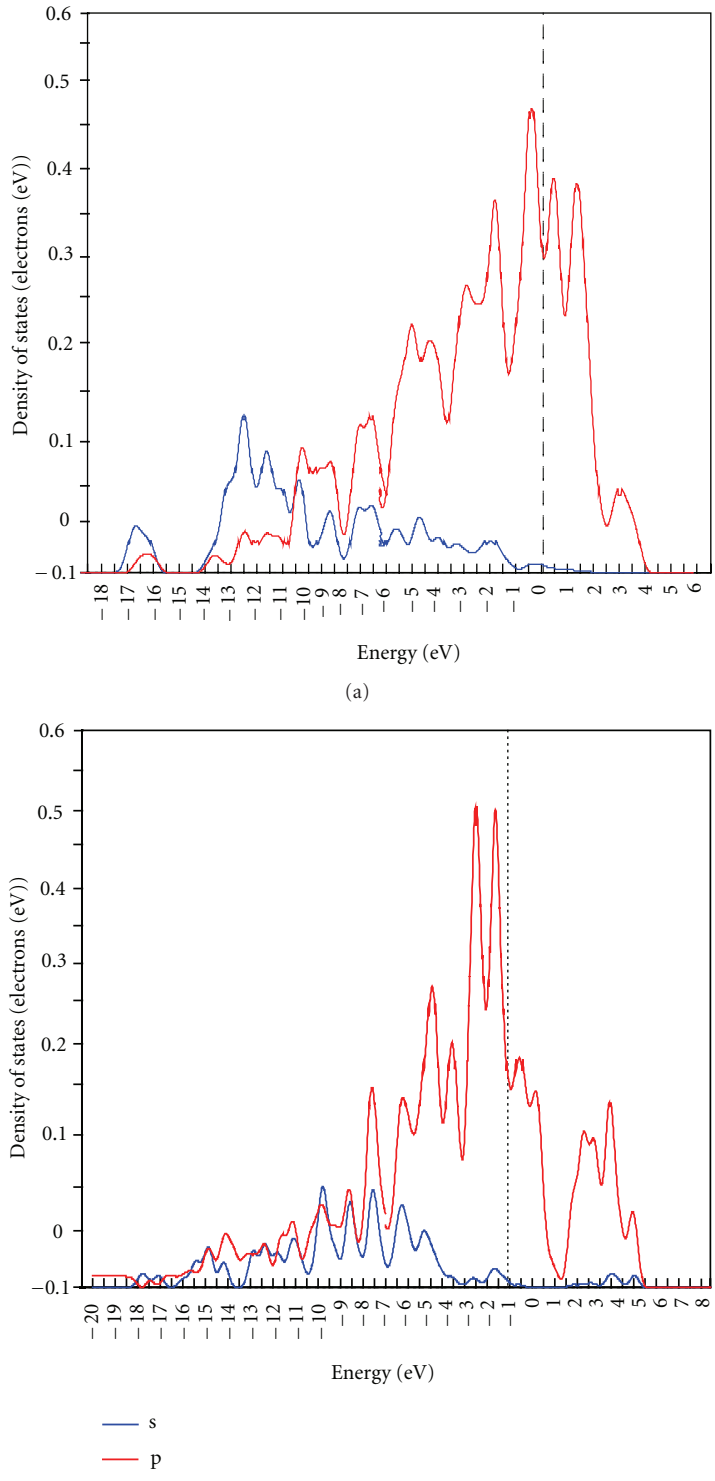

Figure 5: Partial density of states (PDOS) of B atoms of (8,0) (a) BC_3 and (b) B_3C systems.

compute the dielectric constant for parallel, perpendicular polarization and unpolarized one with normal incidence (1,0,0). The parallel polarization refers here to the direction of light parallel to the axis of respective SWCNTs. In Figure 5, we schematically show the dielectric constant (real) for both pure (8,0), BC_3- and B_3C-doped systems as a function of frequency for unpolarized scheme. It is seen in the numerical computation (not shown in the figure) that, in both cases, the imaginary part of the dielectric constant is always positive throughout the range of frequency. This can be understood

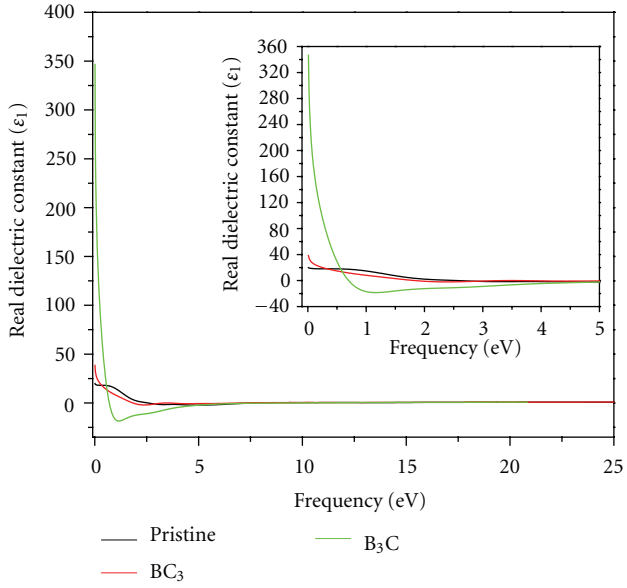

Figure 6: Variation of dielectric constants of pristine (8,0), BC_3 and B_3C under unpolarized scheme. Inset: the variation is shown up to 5 eV.

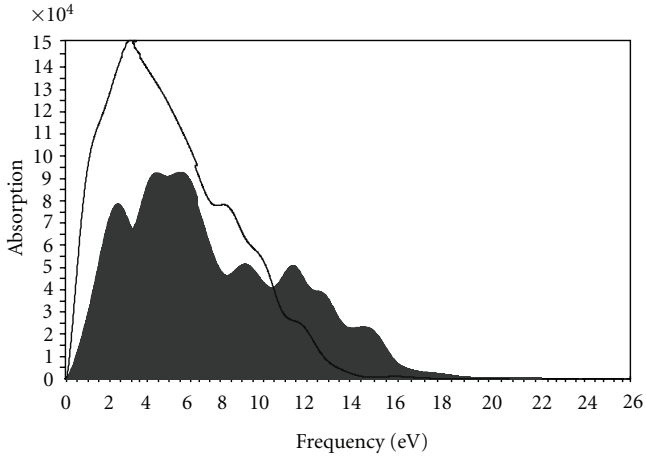

Figure 7: Variation of absorption coefficient (computed in unit of cm^{-1}) with frequency (calculated in energy unit of eV) of BC_3 (shaded) and B_3C.

very simply from (1) used for the numerical simulation study. The square of the matrix element and the even functional nature of the energy conserving delta function ensure the positivity of ε_2. This property of ε_2 serves as one of the crosschecks in our numerical computation.

However, as evident from the figure itself, such a restriction is not obeyed by the real part of the dielectric constant ε_1. We also note that the static value (strictly speaking $\omega \to 0$ but in our numerical computation $\omega = 0.0150$ Hz.) of the dielectric constants for both pure and doped systems is always positive. This observation is further satisfied by a theorem in continuous media stating that the static electric dielectric constant is always positive [35] for any material in thermal equilibrium. The variation of static

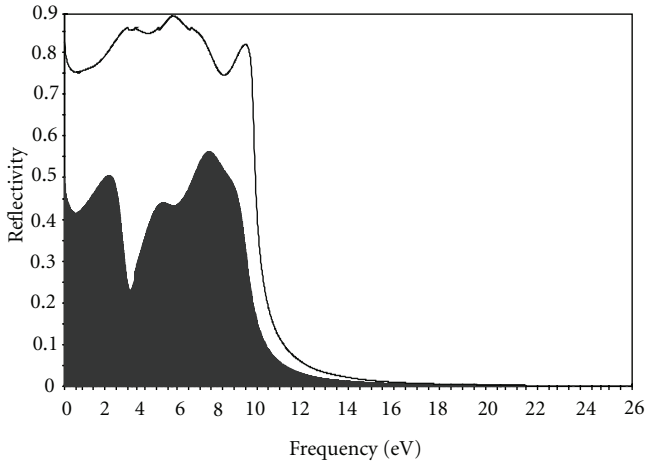

Figure 8: Variation of reflectivity at normal incidence for BC_3 (shaded one) and B_3C for parallel polarization as a function of frequency.

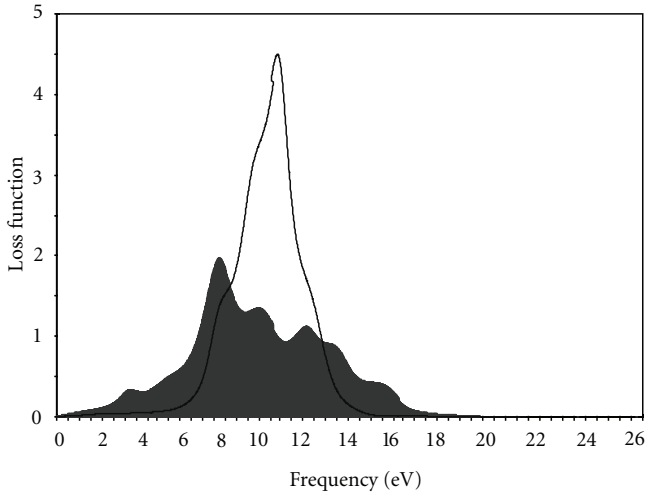

Figure 9: Loss function for BC_3 (shaded) B_3C one for unpolarized case.

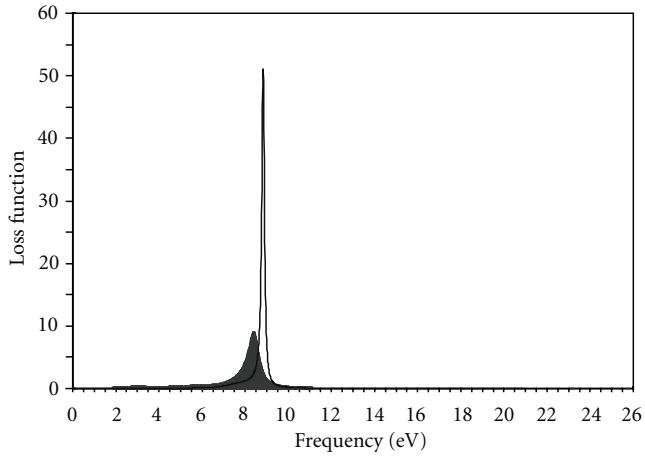

Figure 10: Loss function for BC_3 and B_3C (shaded) for parallel polarization.

dielectric constant with concentration of B has been reported recently [36] to show that a small concentration is enough to change the value drastically from the pure (8,0) SWCNT. It is evident from Figure 6 that the static value of the dielectric constant (real as well as imaginary) of BC_3 system is higher compared to pure one. It has been observed that the static dielectric constant of B_3C is higher than that of BC_3 for any type of polarizations (see Table 1).

In case of semiconducting SWCNT, an *ab initio* tight-binding calculation [37–39] relates the static value of the dielectric constant with the energy band gap as

$$\varepsilon_1(0) = 1 + \frac{\left(\hbar\omega_p\right)^2}{\left(5.4E_g\right)^2}. \quad (3)$$

Here ω_p is the plasma frequency and E_g is the energy band gap. Our numerical calculations are in qualitative agreement with the higher value of the dielectric constant B_3C compared to BC_3 one. In particular, the static dielectric constant in the long wave length limit for B_3C system is 9 times larger than that of BC_3 in unpolarized electromagnetic field with normal incidence (1,0,0).

3.3. Study of the Absorption Spectra of the Doped System. The absorption coefficient α is related to the imaginary part of the dielectric constant as

$$\alpha = \frac{\varepsilon_2\omega}{nc}, \quad (4)$$

where n and c are the refractive index and the speed of light, respectively. The absorption spectra depend critically on the nature of CNT as well as the direction of polarization. The absorption spectra are limited to UV region only.

The existence of peaks in the spectra indicates the maximum absorption at that particular energy. With doping by B atom(s), both the magnitude of the peaks and its position change significantly. We depict, in Figure 7, a comparative study of the absorption coefficient of BC_3 and B_3C systems as a function of frequency in the unpolarized case with normal incidence (1,0,0). We notice that in contrast to B_3C, there exist several peaks in the absorption spectra. The existence of these rich absorption peaks in the overall frequency range is consistent with the theoretical tight-binding calculations made on (3,3) and (6,0) BC_3 nanotubes [40]. It is also evident from the figure that up to 10 eV or so (frequency measured in units of energy), the absorption coefficient of B_3C is always higher than that of BC_3. However, above 10 eV, the reverse is true.

3.4. Study of the Reflectivity at Normal Incidence of the Doped System. The reflectivity $R(\omega)$ of any media at normal incidence is calculated from the refractive indexes via the relations (as implemented in CASTEP [25]) given by

$$R(\omega) = \left(\frac{1-\sqrt{\varepsilon(\omega)}}{1+\sqrt{\varepsilon(\omega)}}\right)^2, \quad \varepsilon(\omega) = \varepsilon_1(\omega) + i\varepsilon_2(\omega). \quad (5)$$

It is clearly evident from the definition that the reflectivity is always positive in the scheduled range of the frequency and is dimensionless. R is sometimes regarded as the index of refraction as a function of wavelength of light used. In Figure 8, we show the variation of reflectivity of BC_3 and B_3C systems for parallel polarization as a function of frequency. It is clear from the figure that the reflectivity of B_3C system is always higher than that of BC_3 in the whole range of frequency. This could be helpful in designing optical devices involving B-doped SWCNT.

3.5. Study of the Loss Function of the Doped System. In this time-dependent calculation of the ground state electronic states, the interaction is between the photon and electrons. The transitions between the occupied and unoccupied states are caused by the electric field of the photon. When these excitations are collective in nature, they are termed as plasmons. The loss function, which is a direct measure of the collective excitations of the systems, is defined as $\mathrm{Im}[-1/\varepsilon(q,\omega)]$. Since we are taking $q \to 0$ limit in our calculation, therefore, we are considering the loss function behavior under the long wavelength limit. The peak position of this loss function determines the typical energy of the plasmons in the system. High-resolution transmission electron microscopy (HRTEM) and nanoelectron energy loss spectroscopy (nano-EELS) can provide information about the systematic and atomic structural defects of B-doped SWCNTs [41–43]. The spectra resulting from these collective excitations can be alternatively understood as a joint DOS between VB and CB weighted by appropriate matrix elements. In terms of the real and imaginary dielectric constants, a straightforward algebra reveals that $\mathrm{Im}[-1/\varepsilon(q,\omega)] = (\varepsilon_2(\omega)/\varepsilon_1^2(\omega) + \varepsilon_2^2(\omega))$. At the plasma frequency, the above expression attains the higher value when $\varepsilon_1 \to 0$ and $\varepsilon_2 < 1$.

In Figures 9 and 10, we depict the anisotropic signature of BC_3 and B_3C systems for unpolarized case and parallel polarization, respectively. For unpolarized case, we notice that within the range of frequency (7–12 eV), the loss function of BC_3 is smaller than that of B_3C. However, above 12 eV, the loss function of BC_3 is higher than that of B_3C. Besides, the main peak of BC_3 at 7.24 eV is seen to shift to 9.89 eV with significantly higher magnitude. While in parallel polarization as evident from Figure 10, the single peak of B_3C at 8.39 eV is shifted to 8.81 eV for BC_3 system with significantly six orders of magnitude. In Table 1, we summarize the main results of the two systems.

4. Conclusions and Perspectives

From the first-principles relaxed C–C bond length DFT calculation of the optical property of BC_3 and B_3C (8,0) SWNT systems, we have observed significant changes in the optical behavior for different polarizations. The behavior of the static dielectric constant of B-doped system depends on the flavor (nature) of the CNTs. The anisotropy signatures of the dielectric constants noticed in these systems are due to the confined geometry of the CNTs. The electronic band structure reveals that the Fermi energy of B_3C system is reduced compared to BC_3. The static dielectric constant in

the long wavelength limit for B_3C system is 9 times larger than that of BC_3 in unpolarized electromagnetic field with normal incidence (1,0,0). Within 10 eV frequency (energy) range, the absorption coefficient of B_3C is higher compared to BC_3, while, above 10 eV, it is less than that of BC_3. In parallel polarization, the peak of the loss function for B_3C is shifted to higher-frequency (energy) region with significantly six orders of magnitude compared to BC_3 system. All these facts about these two systems may throw some light on the nature of collective excitations and nanoscale optical devices.

Acknowledgment

One of the authors (D. Jana) would like to thank the National Science Council (NSC) of Republic of China (R.O.C) for financially supporting him as a visiting researcher under Contract no. NSC 099-2912-I-002-160.

References

[1] R. Saito, G. Dresselhaus, and M. S. Dresselhaus, *Physical Properties of Carbon Nanotubes*, Imperial College Press, London, UK, 1998.

[2] S. Reich, C. Thomsen, and J. Maulzsch, *Carbon Nanotubes: Basic Concepts and Physical Properties*, Wiley-VCH, Weinheim, Germany, 2004.

[3] M. Machón, S. Reich, C. Thomsen, D. Sánchez-Portal, and P. Ordejón, "Ab initio calculations of the optical properties of 4-Å-diameter single-walled nanotubes," *Physical Review B*, vol. 66, no. 15, Article ID 155410, 2002.

[4] X. P. Yang, H. M. Weng, and J. Dong, "Optical properties of 4 Å single-walled carbon nanotubes inside the zeolite channels studied from first principles calculations," *European Physical Journal B*, vol. 32, no. 3, pp. 345–350, 2003.

[5] H. J. Liu and C. T. Chan, "Properties of 4 Å carbon nanotubes from first-principles calculations," *Physical Review B*, vol. 66, no. 11, Article ID 115416, 2002.

[6] G. Y. Guo, K. C. Chu, D.-S. Wang, and C.-G. Duan, "Linear and nonlinear optical properties of carbon nanotubes from first-principles calculations," *Physical Review B*, vol. 69, no. 20, Article ID 205416, 2004.

[7] N. Hamada, S. I. Sawada, and A. Oshiyama, "New one-dimensional conductors: graphitic microtubules," *Physical Review Letters*, vol. 68, no. 10, pp. 1579–1581, 1992.

[8] H. Yokomichi, M. Matoba, T. Fukuhara, H. Sakima, F. Sakai, and K. Maezawa, "Are boron-doped carbon nanotubes metallic?" *Physica Status Solidi (B)*, vol. 207, no. 1, pp. R1–R2, 1998.

[9] J. Kong, N. R. Franklin, C. Zhou et al., "Nanotube molecular wires as chemical sensors," *Science*, vol. 287, no. 5453, pp. 622–625, 2000.

[10] S. Peng and K. Cho, "Ab initio study of doped carbon nanotube sensors," *Nano Letters*, vol. 3, no. 4, pp. 513–517, 2003.

[11] R. Wang, D. Zhang, Y. Zhang, and C. Liu, "Boron-doped carbon nanotubes serving as a novel chemical sensor for formaldehyde," *Journal of Physical Chemistry B*, vol. 110, no. 37, pp. 18267–18271, 2006.

[12] O. Stephan, P. M. Ajayan, C. Colliex et al., "Doping graphitic and carbon nanotube structures with boron and nitrogen," *Science*, vol. 266, no. 5191, pp. 1683–1685, 1994.

[13] Z. Weng-Sieh, K. Cherrey, N. G. Chopra et al., "Synthesis of $B_xC_yN_z$ nanotubules," *Physical Review B*, vol. 51, no. 16, pp. 11229–11232, 1995.

[14] W. Q. Han, J. Cumings, X. Huang, K. Bradley, and A. Zettl, "Synthesis of aligned $B_xC_yN_z$z nanotubes by a substitution-reaction route," *Chemical Physics Letters*, vol. 346, no. 5-6, pp. 368–372, 2001.

[15] E. Borowiak-Palen, T. Pichler, G. G. Fuentes et al., "Efficient production of B-substituted single-wall carbon nanotubes," *Chemical Physics Letters*, vol. 378, no. 5-6, pp. 516–520, 2003.

[16] E. Borowiak-Palen, T. Pichler, A. Graff, R. J. Kalenczuk, M. Knupfer, and J. Fink, "Synthesis and electronic properties of B-doped single wall carbon nanotubes," *Carbon*, vol. 42, no. 5-6, pp. 1123–1126, 2004.

[17] X. Yang, L. Chen, Z. Shuai, Y. Liu, and D. Zhu, "Charge-transport behavior in aligned carbon nanotubes: a quantum-chemical investigation," *Advanced Functional Materials*, vol. 14, no. 3, pp. 289–295, 2004.

[18] T. Picher, E. Borowiak-Palen, G. G. Fuentes et al., "Electronic structure and optical properties of boron doped single-wall carbon nanotubes," *AIP Conference Proceedings*, vol. 685, no. 1, pp. 361–365, 2003.

[19] S. Latil, S. Roche, D. Mayou, and J.-C. Charlier, "Mesoscopic transport in chemically doped carbon nanotubes," *Physical Review Letters*, vol. 92, no. 25, Article ID 256805, 2004.

[20] Y. Liu and H. Guo, "Current distribution in B- and N-doped carbon nanotubes," *Physical Review B*, vol. 69, no. 11, Article ID 115401, 2004.

[21] D. L. Carroll, P. Redlich, X. Blase et al., "Effects of nanodomain formation on the electronic structure of doped carbon nanotubes," *Physical Review Letters*, vol. 81, no. 11, pp. 2332–2335, 1998.

[22] R. Czerw, M. Terrones, J. C. Charlier et al., "Identification of electron donor states in N-doped carbon nanotubes," *Nano Letters*, vol. 1, no. 9, pp. 457–460, 2001.

[23] Y. Miyamoto, A. Rubio, S. G. Louie, and M. L. Cohen, "Electronic properties of tubule forms of hexagonal BC_3 ," *Physical Review B*, vol. 50, no. 24, pp. 18360–18366, 1994.

[24] G. G. Fuentes, E. Borowiak-Palen, M. Knupfer et al., "Formation and electronic properties of BC_3 single-wall nanotubes upon boron substitution of carbon nanotubes," *Physical Review B*, vol. 69, no. 24, Article ID 245403, 2004.

[25] M. D. Segall, P. J. D. Lindan, M. J. Probert et al., "First-principles simulation: ideas, illustrations and the CASTEP code," *Journal of Physics Condensed Matter*, vol. 14, no. 11, pp. 2717–2744, 2002.

[26] D. Jana, L.-C. Chen, C. W. Chen, S. Chattopadhyay, and K.-H. Chen, "A first principles study of the optical properties of B_xC_y single wall nanotubes," *Carbon*, vol. 45, no. 7, pp. 1482–1491, 2007.

[27] D. Jana, L. C. Chen, C. W. Chen, and K. H. Chen, "Ab-initio study of optical conductivity of B_xC_y nano-composite system," *Indian Journal of Physics*, vol. 81, no. 1, pp. 41–45, 2007.

[28] D. Jana, L.-C. Chen, C. W. Chen, and K.-H. Chen, "On refractive index and reflectivity of B_xC_y single wall nanotubes: a first principles approach," *Asian Journal of Physics*, vol. 17, p. 105, 2007.

[29] H. J. Monkhorst and J. D. Pack, "Special points for Brillouin-zone integrations," *Physical Review B*, vol. 13, no. 12, pp. 5188–5192, 1976.

[30] M. C. Payne, M. P. Teter, D. C. Allan, T. A. Arias, and J. D. Joannopoulos, "Iterative minimization techniques for ab initio total-energy calculations: molecular dynamics and

conjugate gradients," *Reviews of Modern Physics*, vol. 64, no. 4, pp. 1045–1097, 1992.

[31] V. Milman, B. Winkler, J. A. White et al., "Electronic structure, properties, and phase stability of inorganic crystals: a pseudopotential plane-wave study," *International Journal of Quantum Chemistry*, vol. 77, no. 5, pp. 895–910, 2000.

[32] J. P. Perdew, K. Burke, and M. Ernzerhof, "Generalized gradient approximation made simple," *Physical Review Letters*, vol. 77, no. 18, pp. 3865–3868, 1996.

[33] K. Liu, P. Avouris, R. Martel, and W. K. Hsu, "Electrical transport in doped multiwalled carbon nanotubes," *Physical Review B*, vol. 63, no. 16, Article ID 161404, 2001.

[34] B. Wei, R. Spolenak, P. Kohler-Redlich, M. Rühle, and E. Arzt, "Electrical transport in pure and boron-doped carbon nanotubes," *Applied Physics Letters*, vol. 74, no. 21, pp. 3149–3151, 1999.

[35] L. D. Landau and E. M. Lifshitz, *Electrodynamics of Continuous Media*, Pergamon Press, New York, NY, USA, 1984.

[36] L. X. Benedict, S. G. Louie, and M. L. Cohen, "Static polarizabilities of single-wall carbon nanotubes," *Physical Review B*, vol. 52, no. 11, pp. 8541–8549, 1995.

[37] T. Pichler, M. Knupfer, M. S. Golden, J. Fink, A. Rinzler, and R. E. Smalley, "Localized and delocalized electronic states in single-wall carbon nanotubes," *Physical Review Letters*, vol. 80, no. 21, pp. 4729–4732, 1998.

[38] M. Ouyang, J. L. Huang, C. L. Cheung, and C. M. Lieber, "Energy gaps in "Metallic" single-walled carbon nanotubes," *Science*, vol. 292, no. 5517, pp. 702–705, 2001.

[39] R. Krupke, F. Hennrich, H. V. Löhneysen, and M. M. Kappes, "Separation of metallic from semiconducting single-walled carbon nanotubes," *Science*, vol. 301, no. 5631, pp. 344–347, 2003.

[40] S. C. Chen, I. Y. Chen, Y. H. Ho, and M. F. Lin, "Optical properties of BC_3 nanotubes," *Journal of Vacuum Science and Technology B*, vol. 24, no. 1, pp. 46–49, 2006.

[41] P. L. Gai, O. Stephan, K. McGuire et al., "Structural systematics in boron-doped single wall carbon nanotubes," *Journal of Materials Chemistry*, vol. 14, no. 4, pp. 669–675, 2004.

[42] A. Graft, T. Gemming, E. Borowiak-Palen et al., "Analytical TEM investigations of B-doped carbon and BN nanotubes," *Microscopy and Microanalysis*, vol. 9, supplement 3, pp. 178–179, 2003.

[43] E. Borowiak-Palen, T. Pichler, G. G. Fuentes et al., "Production and characterization of MWBNNT and B-doped SWCNT," *AIP Conference Proceedings*, vol. 685, no. 1, pp. 374–377, 2003.